

# Supplemental Information: The Impacts of Dopants on the Small Polaron Carrier Mobility and Conductivity in Hematite - The Role of Disorder

Mingpeng Chen,<sup>†,§</sup> Andrew C. Grieder,<sup>†,§</sup> Tyler J. Smart,<sup>‡,¶</sup> Kiley Mayford,<sup>‡</sup>  
Samuel McNair,<sup>‡</sup> Anica Pinongcos,<sup>†</sup> Samuel Eisenberg,<sup>†</sup> Frank Bridges,<sup>‡</sup> Yat Li,<sup>†</sup>  
and Yuan Ping<sup>\*,†</sup>

<sup>†</sup>*Department of Chemistry and Biochemistry, University of California, Santa Cruz, CA, 95064,  
USA*

<sup>‡</sup>*Department of Physics, University of California, Santa Cruz, CA, 95064, USA*

<sup>¶</sup>*Lawrence Livermore National Laboratory, Livermore, California 94551, USA*

<sup>§</sup>*Contributed equally to this work*

E-mail: yuanping@ucsc.edu

## Kinetic Monte Carlo Sampling Calculations

First, the diffusion coefficient is obtained by fitting mean square displacement (MSD) over time as shown in Eq. 1,

$$D = \lim_{t \rightarrow \infty} \frac{\langle MSD(t)^2 \rangle}{2Nt} \quad (1)$$

where  $D$  is the diffusion coefficient,  $t$  is time, and  $N$  is the number of dimensions. Here  $N$  is 2 since only diffusion in the a-b plane is considered. In order to calculate MSD using kinetic Monte Carlo (kMC) simulations, non-equivalent electron transfer rates  $k_{ab}$  are calculated for all nearest neighbor hoppings using Eq. 2.

$$k_{ab} = \tau_0 e^{\frac{-E_a^{ab}}{k_B T}} \quad (2)$$

where  $E_a^{ab}$  is the activation energy for  $EP$  hopping from site a to b,  $\tau_0$  is the attempt frequency listed in Table S4,  $k_B$  is the Boltzmann constant, and  $T$  is temperature. The MSD is calculated using the distance from a to b and the time step of the hop which is determined from the electron transfer rate from site a to b, as explained in the SI of Ref. 1. To ensure convergence of the MSD from kMC simulations, each of the MSD was averaged from 16 individual runs with each sampled 12800 times. Convergence is confirmed by comparing simulation sampled 100, 1200, and 12800 times as seen in Fig. S1. Second, the same procedure was repeated at various temperatures to obtain diffusion coefficients at 400, 500, 600, 700, 800, 900, 1000, 1250, and 1500 K. The effective barrier was then determined by fitting the slope of the Arrhenius relation of diffusion coefficients and temperature from Eq. 3,

$$D = D_0 e^{\frac{-E_a}{k_B T}} \quad (3)$$

where  $D_0$  is the diffusion pre-factor,  $E_a$  is the effective activation energy barrier,  $k_B$  is the Boltz-

mann constant, and  $T$  is temperature.

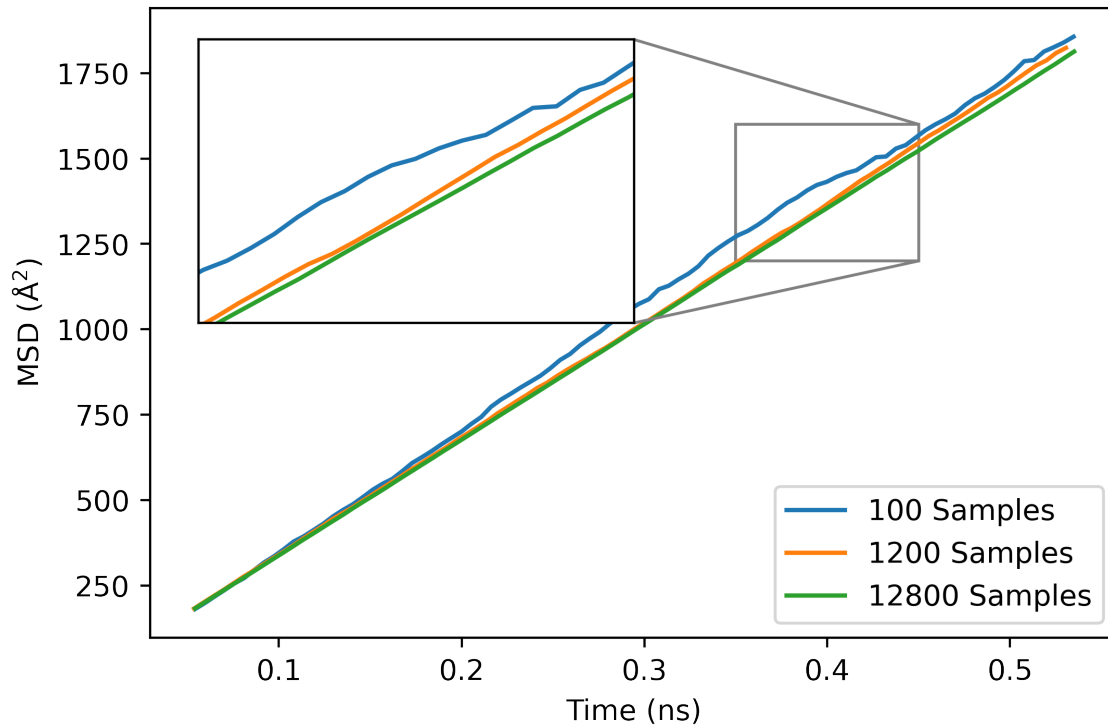


**Figure S1.** Mean Square Displacement (MSD) over time for kMC simulations of layer 5 in the Nb doped system at 300K. "Samples" means the number of times the kMC was sampled (this is same as "N" defined in the SI of Ref. 1). We performed calculations with the same procedure for other layers and dopants (not shown here).

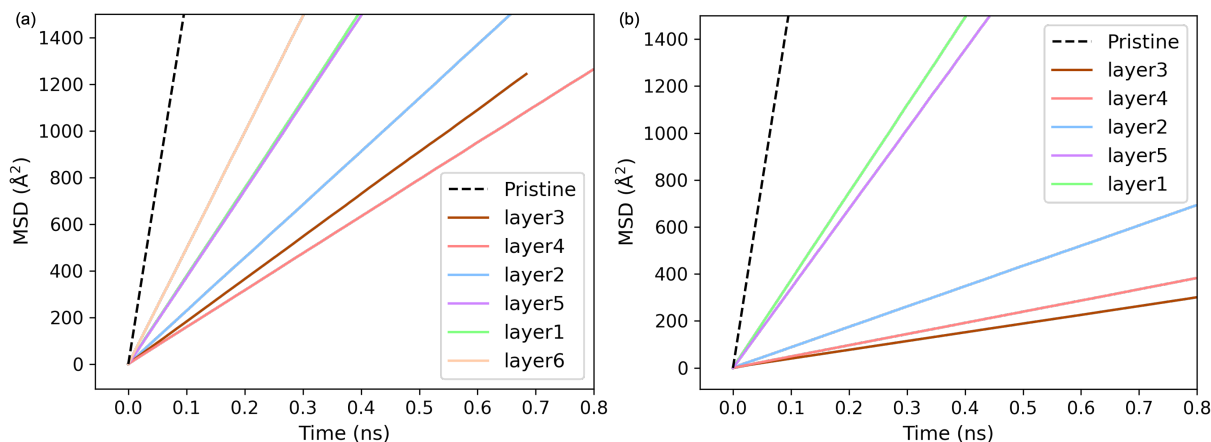


**Figure S2.** Mean Squared Displacement (MSD) over time at different layers (ab planes) from kinetic Monte Carlo (kMC) simulations after averaging over 16 kMC simulations. After the dashed line for pristine, the legend is in order of increasing distance to dopant a) Ti doped b) Nb doped. The dopant sits in layer 3.

## Synthesis of Doped $\text{Fe}_2\text{O}_3$ Samples

Doped hematite nanowires were prepared by a two-step process. First,  $\text{FeOOH}$  nanowires were synthesized using a hydrothermal method reported previously.<sup>2</sup> Then  $\text{FeOOH}$  nanowire powders were mixed with dopant precursor solution. The three dopant precursor solutions are tin tetrachloride ( $\text{SnCl}_4$ ) dissolved in ethanol, ammonium niobate(V) oxalate ( $\text{C}_2\text{H}_9\text{NNbO}_6$ ) dissolved in water, and titanium butoxide ( $\text{Ti}(\text{O}i\text{Bu})_4$   $\text{Bu}=\text{CH}_2\text{CH}_2\text{CH}_2\text{CH}_3$ ) dissolved in acidized ethanol (70  $\mu\text{L}$  concentrated  $\text{HCl}$  added into 20 mL ethanol). We adjusted the concentration of the precursor solution to control the doping concentration. The powders were dried at 80° C and then annealed in air at 550° C for 30 min to convert  $\text{FeOOH}$  to hematite. The sample was further annealed at 800° C for another 30 min to facilitate the diffusion of dopants into the hematite crystal structure. The prepared doped hematite samples were used for EXAFS characterization.

## XRD and EXAFS Characterization of Doped $\text{Fe}_2\text{O}_3$

The EXAFS data for the Sn and Nb K edges were collected on beamline 4-1 at the Stanford Synchrotron Radiation Lightsource (SSRL), using 220 Si monochromator crystals. At these edges, the

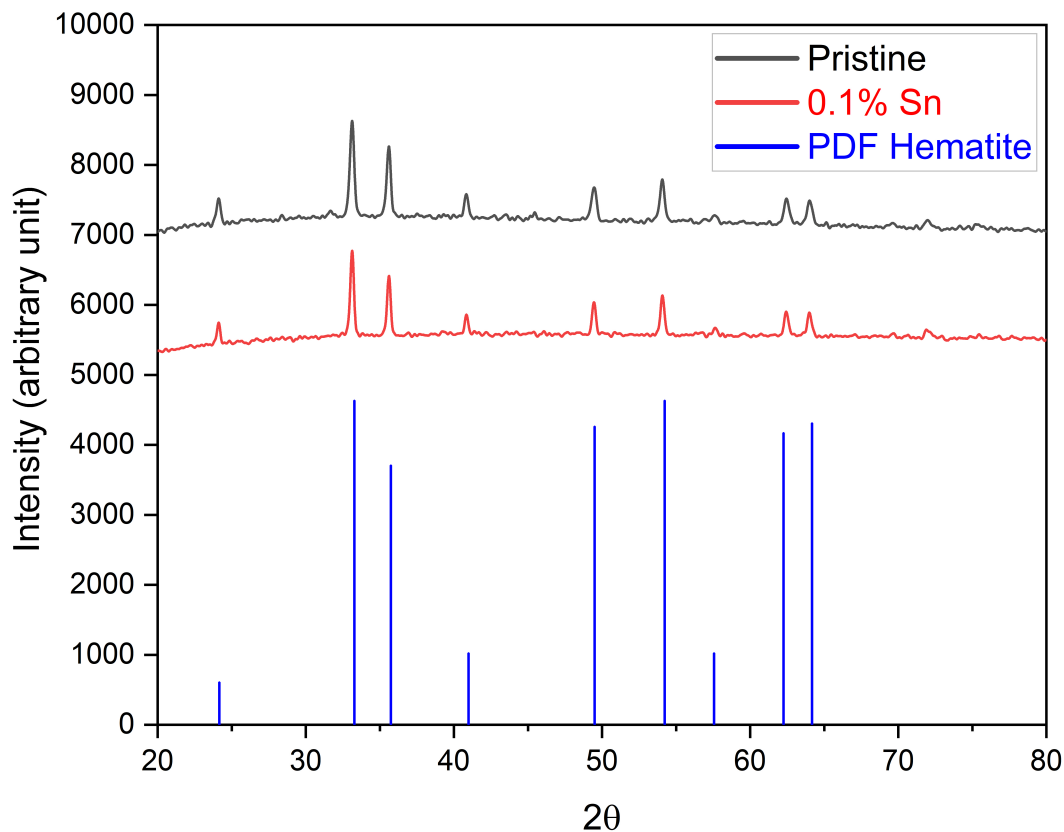


**Figure S3.** Powder X-ray diffraction patterns obtained from pristine hematite (black curve) and 0.1% Sn-doped hematite (red curve). The reported powder data file (PDF) of hematite (PDF# 01-1053) is added for comparison.

monochromator was detuned 30% to reduce harmonics; the slits were  $0.2 \times 6.0 \text{ mm}^2$ , providing an instrumental resolution of  $\approx 3 \text{ eV}$  for Sn and  $1.0 \text{ eV}$  for Nb, well below the core-hole lifetime values. A 30 element Ge fluorescence detector was used to collect the fluorescence data. For the low energy Ti K edge (4966 eV) the data were collected on beamline 4-3, using 111 Si monochromator crystals. Again the monochromator was detuned 30% to reduce harmonics. The slits were  $1 \times 4 \text{ mm}^2$ , providing an instrumental resolution of  $\approx 1 \text{ eV}$ ; a Canberra X-PIPS 7-element silicon drift detector was used to collect the Ti fluorescence. For each data set an Oxford helium cryostat was used to cool the sample to 10 K.

For this comparison we used very low concentration samples with nominally 0.1 % dopant, to

minimize formation of any oxide precipitate. Recent theoretical calculations<sup>3</sup> showed that there is a critical dopant concentration, below which dopant substitution on an Fe site occurs; this critical concentration depends on the temperature at which the samples were made. Because of the low dopant level, measured concentrations in the EXAFS samples were difficult to do and only reliable for Sn (0.07%). For higher concentration samples, measured concentrations were generally in the range of 50-75 % of the nominal value; i.e. for nominal 0.1 % Ti and Nb doped samples, concentrations should be in the range 0.05-0.075 %.

The X-ray data were reduced using the RSXAP,<sup>4</sup> package of programs, which uses standard techniques to remove the pre- and post-backgrounds, and to extract the EXAFS oscillations as a function of  $k$ . Next, a fast Fourier transform (FFT) was used to transform the data to  $r$ -space, as plotted in Figure S4.

To illustrate the significant order about a dopant in these samples, the  $r$ -space data for the Sn dopant are plotted out to 10 Å in Fig. S5. Peaks are visible out to 9.5 Å on this plot (and are present even above 10 Å). The amplitude of the  $r$ -space EXAFS function decreases rapidly with  $r$  because it is weighted by  $1/r^2$ . When this is taken into account, the peak near 9.5 Å is comparable to the nearest neighbor peak - see details in caption.

The data were fit to a sum of pair-functions, calculated using FEFF7<sup>5</sup> for the dopant atom substituted on an Fe site in undistorted Fe<sub>2</sub>O<sub>3</sub>. The initial distances started at the values for hematite. There are six dopant-O and five dopant-Fe peaks out to 4.1 Å. Some of the longer dopant-O peaks had little amplitude and could be omitted, while some of the shorter dopant-O peaks could not be resolved and therefore a single dopant-O peak was used. Finally, one or two small multi-scattering (MS) peaks were included. The Sn fits used 9 peaks, the Nb fits used 8, while the Ti fits used 10. For the current comparison however, we focus on the dopant-O peaks in the first shell and the first main dopant-Fe peak near 3 Å; further neighbor peaks have little influence on these peaks. The shortest dopant-Fe distance (one neighbor near 2.9 Å) is constrained to the larger peak near 3 Å. In the first O shell of hematite there are two Fe-O distances, 1.944 and 2.116 Å. For Sn the two corresponding Sn-O peaks moved together and could not be resolved; and a single function for the

Sn-O peak was used. For Ti and Nb, the splitting of these dopant-O peaks could be resolved and two peaks were used. These results are plotted in the main paper.

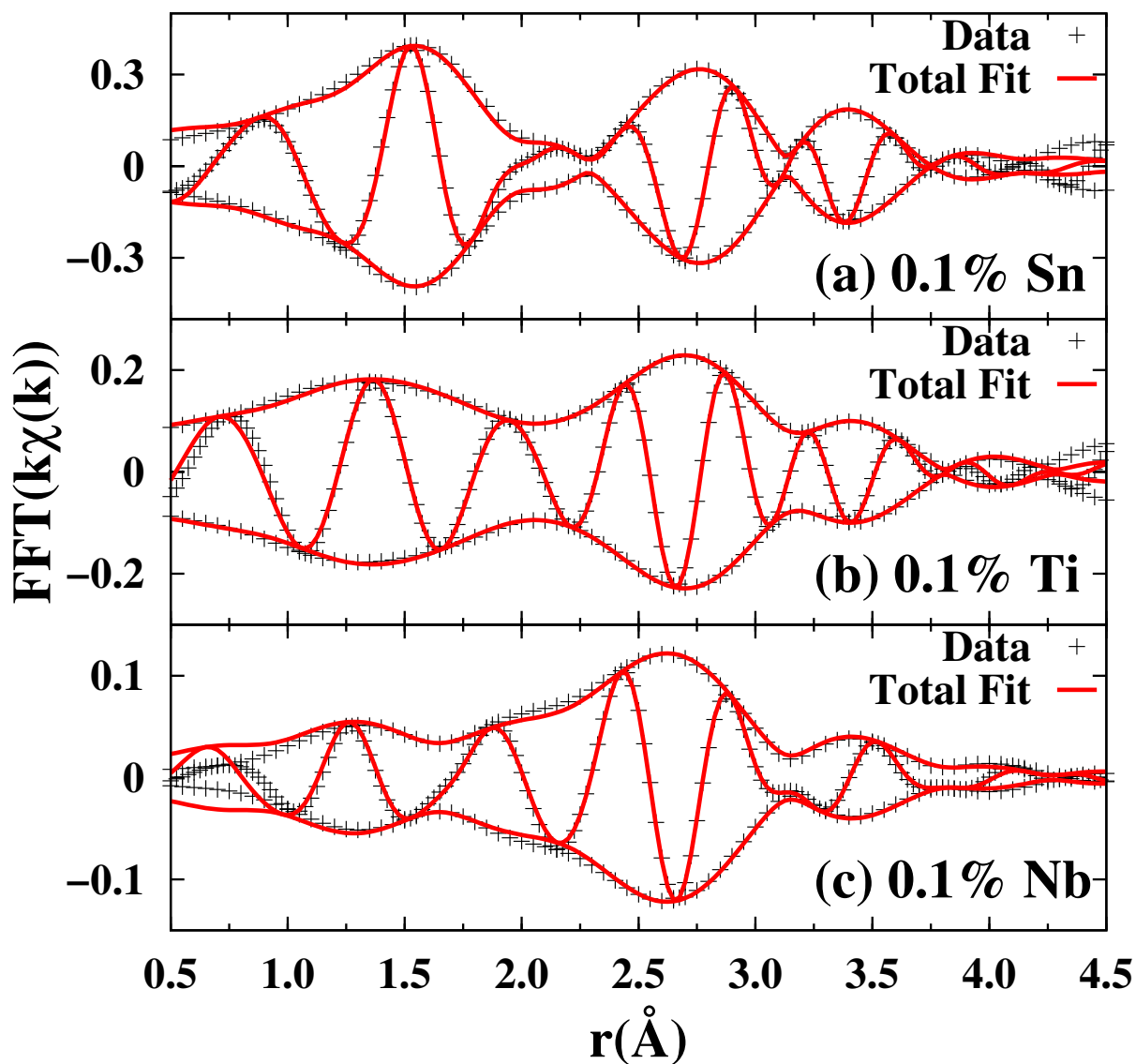


**Figure S4.** EXAFS plots in  $r$ -space for the Sn, Ti, and Nb dopants in hematite. The points are the data and the red line is a fit as described in text. The nominal concentrations are 0.1 %, actual concentrations are in the range 0.05-0.075 %. Fourier transform ranges in  $k$ -space: Sn, 3.5-12  $\text{\AA}^{-1}$ ; Ti, 3.5-10.5  $\text{\AA}^{-1}$ ; Nb, 4-11  $\text{\AA}^{-1}$ . Fit ranges in  $r$ -space: Sn, 1-4  $\text{\AA}$ ; Ti, 1-4 $\text{\AA}$ ; Nb, 1-4.5  $\text{\AA}$ . From these fits the first shell dopant-oxygen and first main dopant-Fe distances are extracted and discussed in main paper.

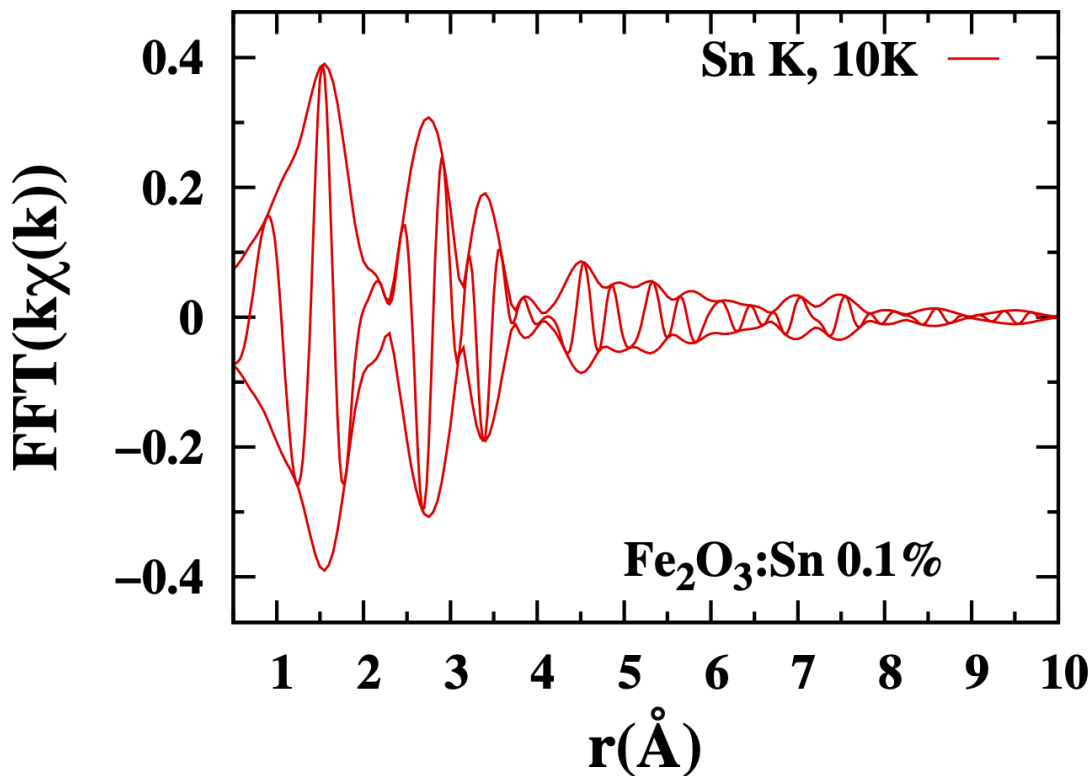


**Figure S5.** The  $r$ -space data at the Sn K edge out to 10 Å for the 0.1 % sample. Peaks are clearly visible out to 10 Å (and even a little beyond). These peak amplitudes are significant and indicate little disorder about the Sn dopant ion. Remember the EXAFS function is weighted by  $1/r^2$ ; when this multiplicative factor is accounted for, the peak at 9.5 Å has a comparable amplitude to that for the nearest neighbor Sn-O peak, and is only a factor of 2.5 smaller than the largest Sn-Fe peak near 3 Å.

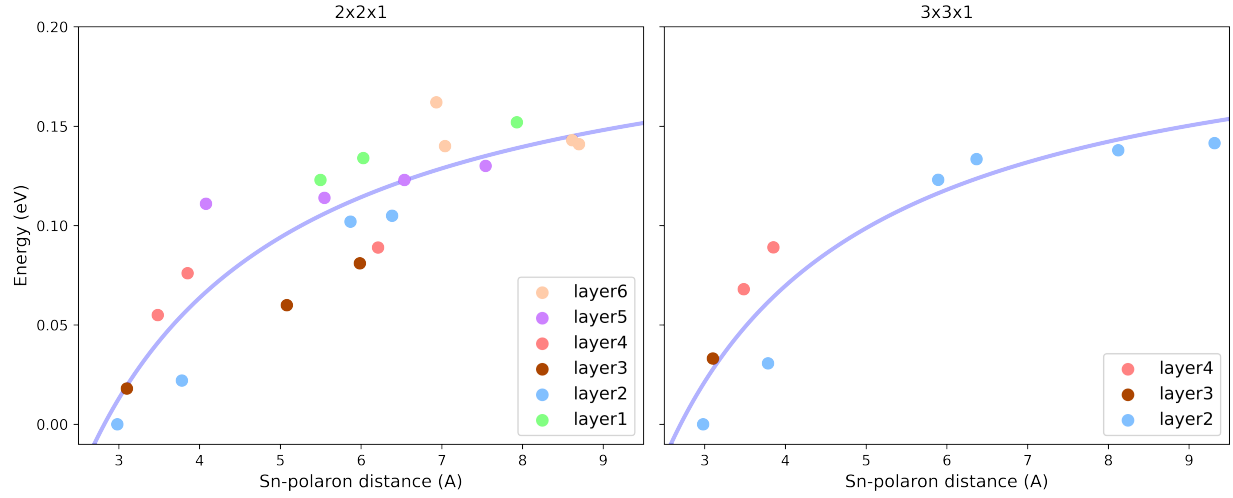


**Figure S6.** Comparison of electron polaron energy as a function of Sn-polaron distance in (a)  $2 \times 2 \times 1$  supercell and (b)  $3 \times 3 \times 1$  supercell. The energy zero is referenced to the lowest energy configuration.

**Table S1.** Reaction energies ( $E_{FS} - E_{IS}$ ) (eV) and activation energies ( $E_a$ ) (eV) of every in-plane *EP* hopping in Sn doped hematite.

Sample	Layer	$FS \rightarrow IS$	$E_{FS} - E_{IS}$ (eV)	$E_a$ (eV)
Prstine	NA	NA	0.00	0.110
Sn	1	1→2	0.011	0.142
Sn	1	1→4	0.029	0.139
Sn	2	1→2	0.022	0.160
Sn	2	2→3	0.080	0.185
Sn	2	3→4	0.003	0.139
Sn	3	1→2	0.043	0.170
Sn	3	2→3	0.020	0.145
Sn	4	1→2	0.022	0.178
Sn	4	2→3	0.013	0.140
Sn	5	1→2	0.003	0.138
Sn	5	2→3	0.009	0.154
Sn	5	3→4	0.007	0.140
Sn	6	2→1	0.022	0.137
Sn	6	2→3	0.003	0.139

**Table S2.** Reaction energies ( $E_{FS} - E_{IS}$ ) (eV) and activation energies ( $E_a$ ) (eV) of every in-plane  $EP$  hopping for Ti doped hematite.

Sample	Layer	$FS \rightarrow IS$	$E_{FS} - E_{IS}$ (eV)	$E_a$ (eV)
Prstine	NA	NA	0.00	0.110
Ti	1	1 $\rightarrow$ 2	0.003	0.141
Ti	1	1 $\rightarrow$ 4	0.033	0.142
Ti	2	1 $\rightarrow$ 2	-0.063	0.092
Ti	2	2 $\rightarrow$ 3	0.070	0.187
Ti	2	3 $\rightarrow$ 4	-0.002	0.138
Ti	3	1 $\rightarrow$ 2	0.026	0.155
Ti	3	2 $\rightarrow$ 3	0.018	0.149
Ti	4	1 $\rightarrow$ 2	0.045	0.179
Ti	4	2 $\rightarrow$ 3	-0.006	0.130
Ti	5	1 $\rightarrow$ 2	0.013	0.146
Ti	5	2 $\rightarrow$ 3	-0.014	0.140
Ti	5	3 $\rightarrow$ 4	0.030	0.165
Ti	6	1 $\rightarrow$ 2	-0.033	0.101
Ti	6	2 $\rightarrow$ 3	0.002	0.135

**Table S3.** Reaction energies ( $E_{FS} - E_{IS}$ ) (eV) and activation energies ( $E_a$ ) (eV) of every in-plane  $EP$  hopping for Nb doped hematite.

Sample	Layer	$FS \rightarrow IS$	$E_{FS} - E_{IS}$ (eV)	$E_a$ (eV)
Prstine	NA	NA	0.00	0.110
Nb	1	1 $\rightarrow$ 2	-0.010	0.129
Nb	1	1 $\rightarrow$ 4	0.031	0.139
Nb	2	1 $\rightarrow$ 2	0.003	0.147
Nb	2	2 $\rightarrow$ 3	0.118	0.210
Nb	2	3 $\rightarrow$ 4	0.00	0.150
Nb	3	1 $\rightarrow$ 2	0.077	0.200
Nb	3	2 $\rightarrow$ 3	0.038	0.148
Nb	4	1 $\rightarrow$ 2	0.064	0.223
Nb	4	2 $\rightarrow$ 3	-0.012	0.130
Nb	5	1 $\rightarrow$ 2	0.022	0.142
Nb	5	2 $\rightarrow$ 3	-0.007	0.150
Nb	5	3 $\rightarrow$ 4	0.040	0.169

**Table S4.** Parameters for carrier mobility calculations in pristine hematite.

Parameters	Values
Electron charge ( $e$ ) (C)	$1.6 \times 10^{-19}$
$EP$ hopping distance ( $a$ ) (cm)	2.83
Equivalent neighbors ( $n$ )	3
Attempt frequency <sup>6</sup> ( $\tau_0$ ) ( $\text{THz}^{-1}$ )	168.9
Thermal energy ( $k_B T$ ) (eV)	0.0259

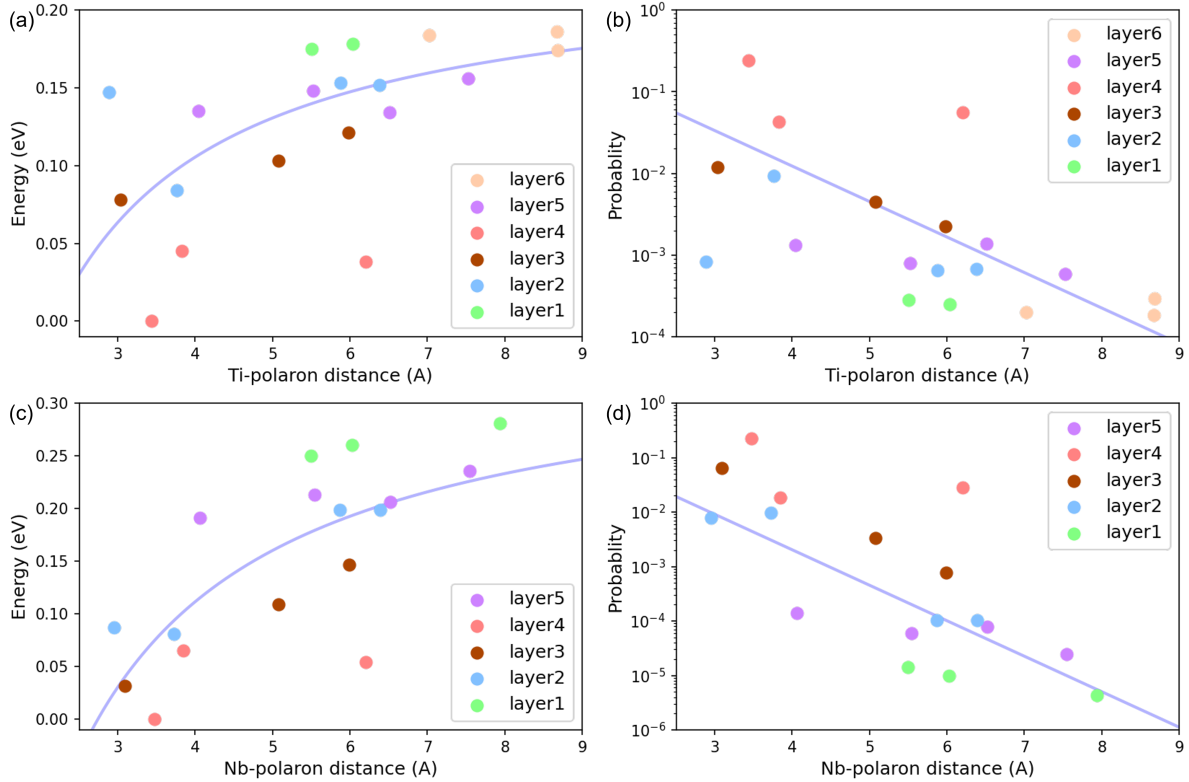


**Figure S7.**  $EP$  energy and probability distribution for Ti and Nb doped hematite. Ti is neutral ( $Q_0$ ) while Nb doped hematite is calculated with one positive charge ( $Q+1$ ) to make sure only one  $EP$  in the supercell. (a)(c) Energy distribution of  $EP$  locating at different Fe sites as a function of Ti-polaron/Nb-polaron distance. The Coulomb interaction trend is highlighted by the curve. (b)(d) Probability distribution of  $EP$  locating at different Fe sites as a function of Ti-polaron/Nb-polaron distance. The line is indicating the reverse relationship between the probability and dopant-polaron distance. Dopant is always substituting the central Fe site in layer 3.

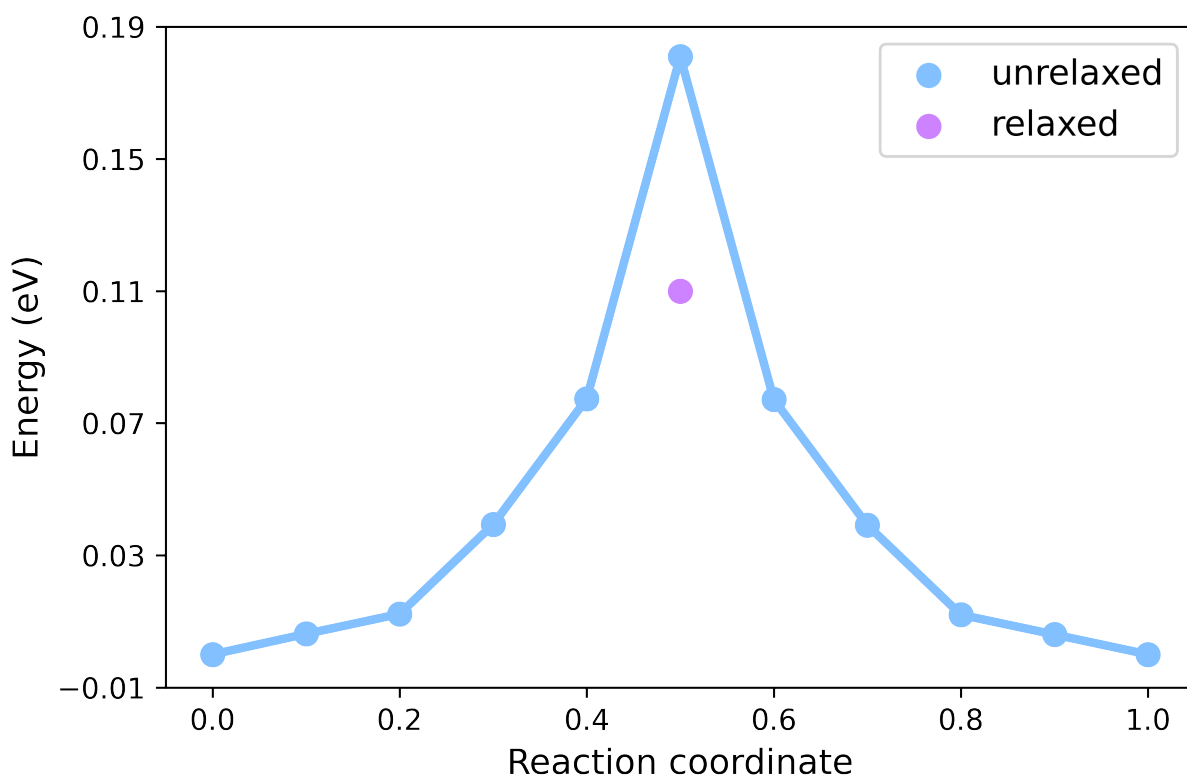


**Figure S8.** The hopping barrier calculated from linear interpolation between initial and final states in pristine hematite. The purple dot is the energy barrier relaxed with the geometry at the highest point while other data points are the energy of intermediate images. The reference zero energy is set with the energy of the initial state. Other barrier calculations of doped systems are done with the same method (not shown).

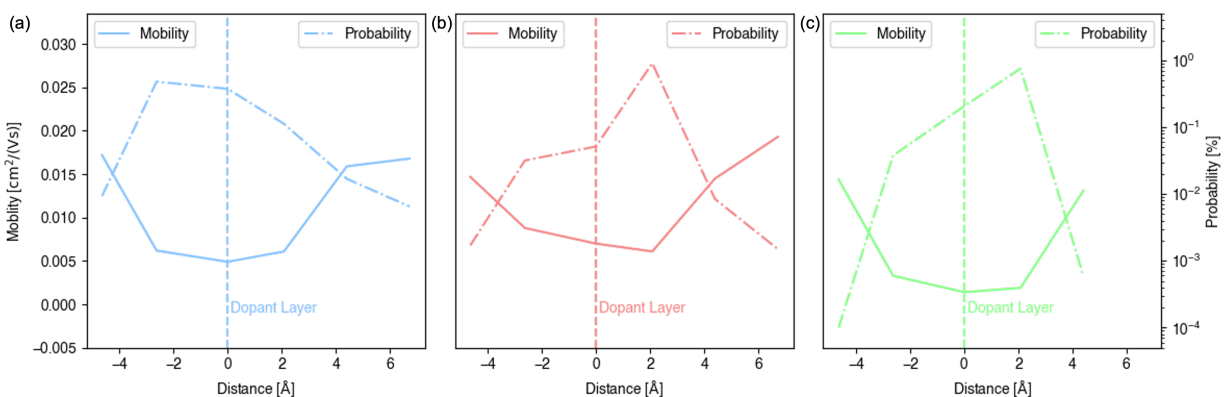


**Figure S9.** Carrier mobility of each layer (solid lines) and probability forming polaron on each layer (dashed lines) for different dopants: a) Sn, b) Ti, and c) Nb. Dopant sits in layer 3, and x-axis is the distance from the dopant layer to other layers along the out-of plane direction. Negative distances denote the ones for layers below dopant.

**Table S5.** The probability of *EP* forming at each layer and carrier mobility ( $\mu_i$ ) in each layer for pristine hematite (only one value due to symmetry) and three different doped hematite.

Layers	Probability	$\mu_i$ (cm <sup>2</sup> /(Vs))
Pristine	–	0.0560
Sn 1	0.0093	0.0172
Sn 2	0.4807	0.0062
Sn 3	0.3744	0.0049
Sn 4	0.1122	0.0061
Sn 5	0.0169	0.0159
Sn 6	0.0065	0.0168
Ti 1	0.0017	0.0147
Ti 2	0.0317	0.0088
Ti 3	0.0514	0.0070
Ti 4	0.9054	0.0061
Ti 5	0.0084	0.0145
Ti 6	0.0015	0.0193
Nb 1	0.0001	0.0144
Nb 2	0.0377	0.0033
Nb 3	0.2063	0.0014
Nb 4	0.7553	0.0019
Nb 5	0.0006	0.0131

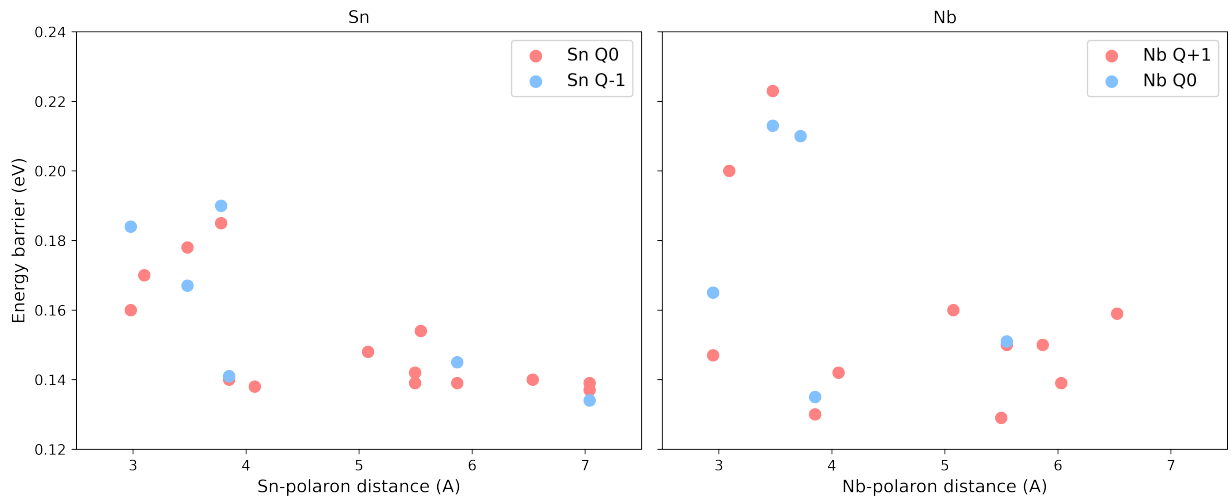


**Figure S10.** *EP* hopping barrier at different dopant charge states for Sn (left panel) and Nb (right panel) doped hematite. Note that for Sn Q-1 and Nb Q0 systems, some energy barriers are missing because *EP* can not be stably formed at certain positions.

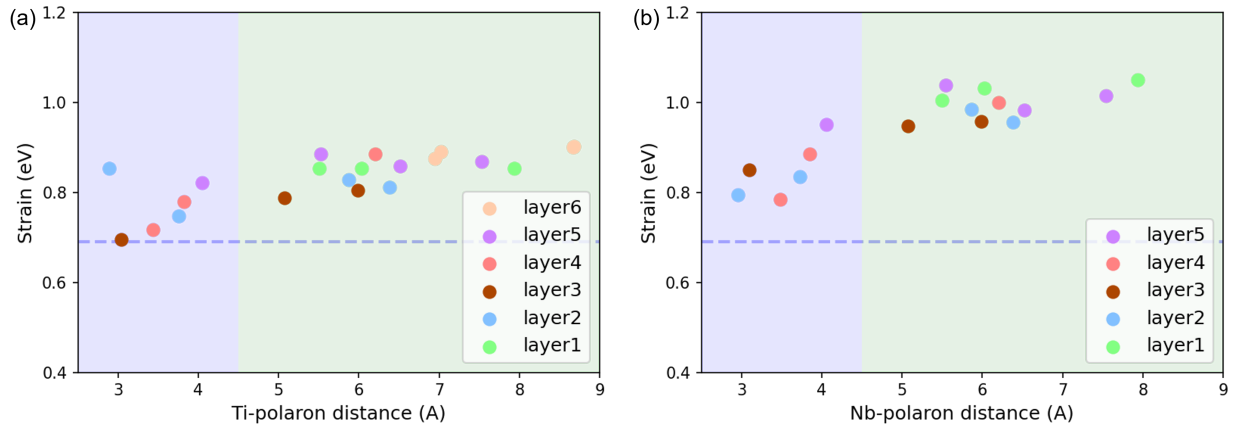


**Figure S11.** Strain energy of *EP* locating at different Fe sites for (a) Ti and (b) Nb doped hematite as a function of dopant-polaron distance in  $2 \times 2 \times 1$  supercells. The dashed line in the plot is the summation of strain energy of isolated Ti/Nb dopant and the one of *EP*. This dashed line represents the limit where the *EP* and dopant are sufficiently far apart (introducing strain to the system independently).

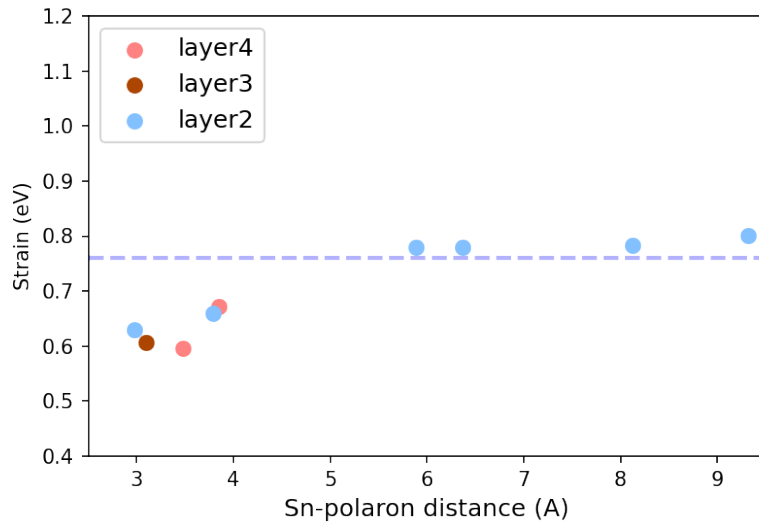


**Figure S12.** Strain energy of *EP* locating on different Fe sites for Sn doped hematite with a  $3 \times 3 \times 1$  supercell. The dashed line in the plot is the summation of strain energy of isolated Sn dopant and the one of *EP*. This dashed line represents the limit where the *EP* and dopant are sufficiently far apart (introducing strain independently).

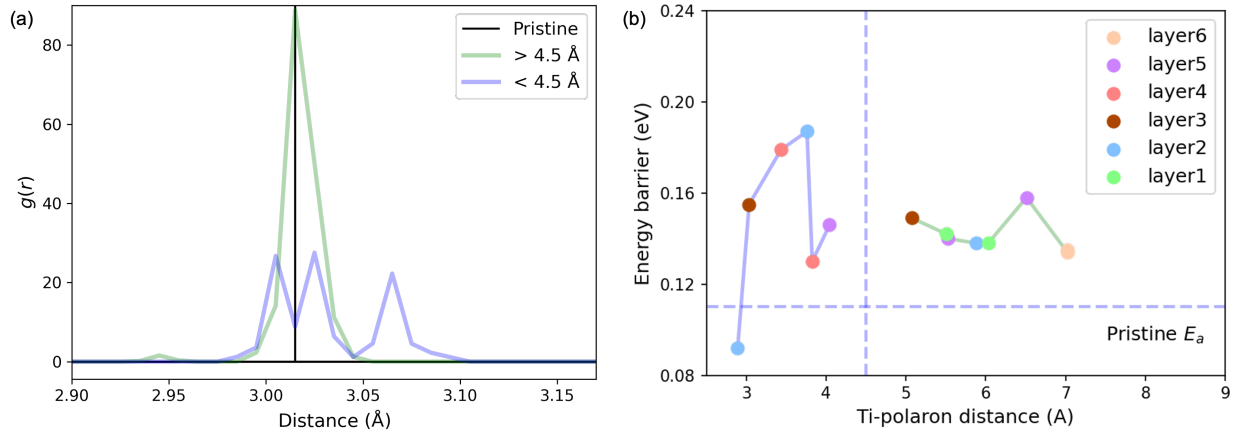


**Figure S13.** Pair distribution function (PDF) and energy barrier as a function of Ti-polaron distance. (a) PDF of Fe-Fe pair distance for Ti dopant with ranges of smaller (purple) or larger (green) than 4.5  $\text{\AA}$ . (b)  $EP$  hopping barriers for Ti doped hematite as a function of Ti-polaron distance. The horizontal dashed line in the plot is the  $EP$  hopping barrier in pristine hematite as a reference.

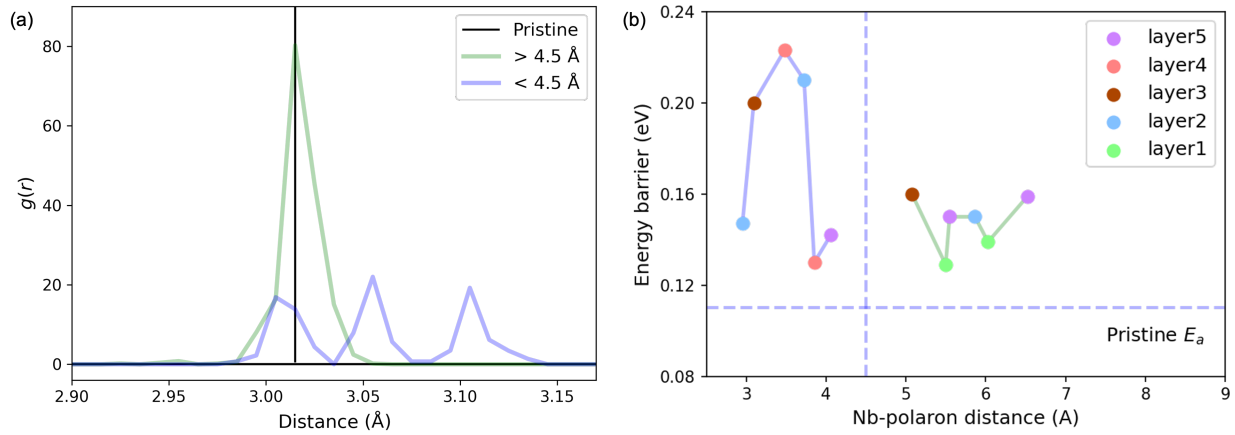


**Figure S14.** Pair distribution function (PDF) and energy barrier as a function of Nb-polaron distance. (a) PDF of Fe-Fe pair distance for Nb dopant with ranges of smaller (purple) or larger (green) than 4.5  $\text{\AA}$ . (b)  $EP$  hopping barriers for Nb doped hematite as a function of Nb-polaron distance. The horizontal dashed line in the plot is the  $EP$  hopping barrier in pristine hematite as a reference.

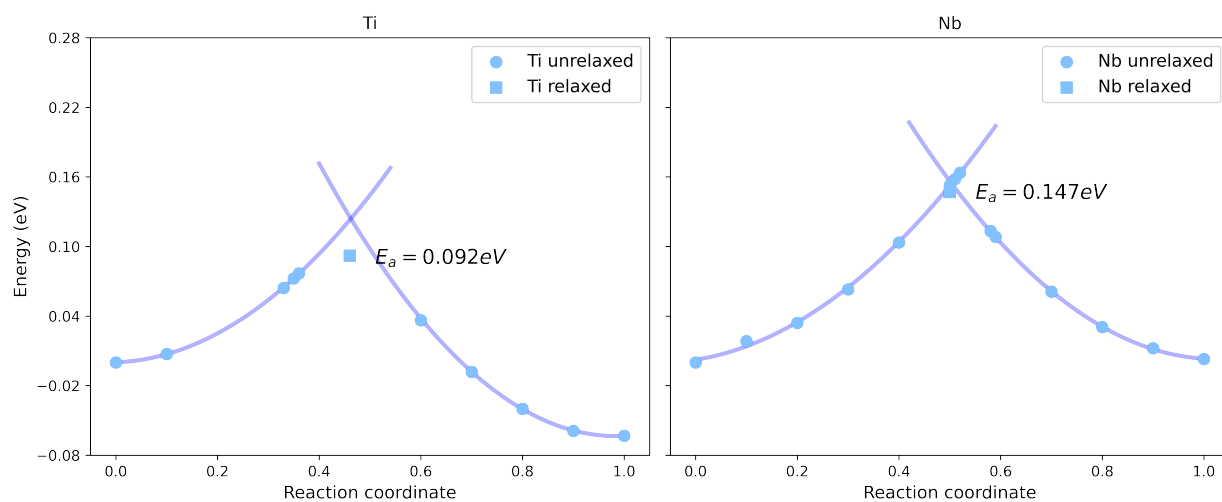


**Figure S15.** Comparison of two selected representative PESs of *EP* hopping. The plot on the left is selected from Ti doped hematite and the right from Nb doped hematite. Although the polaron hopping between left and right panels has similar Fe-Fe distances, the left panel has a smaller barrier (as indicated by  $E_a$ ) than the right panel due to the downward shift of final state's PES in the left panel.

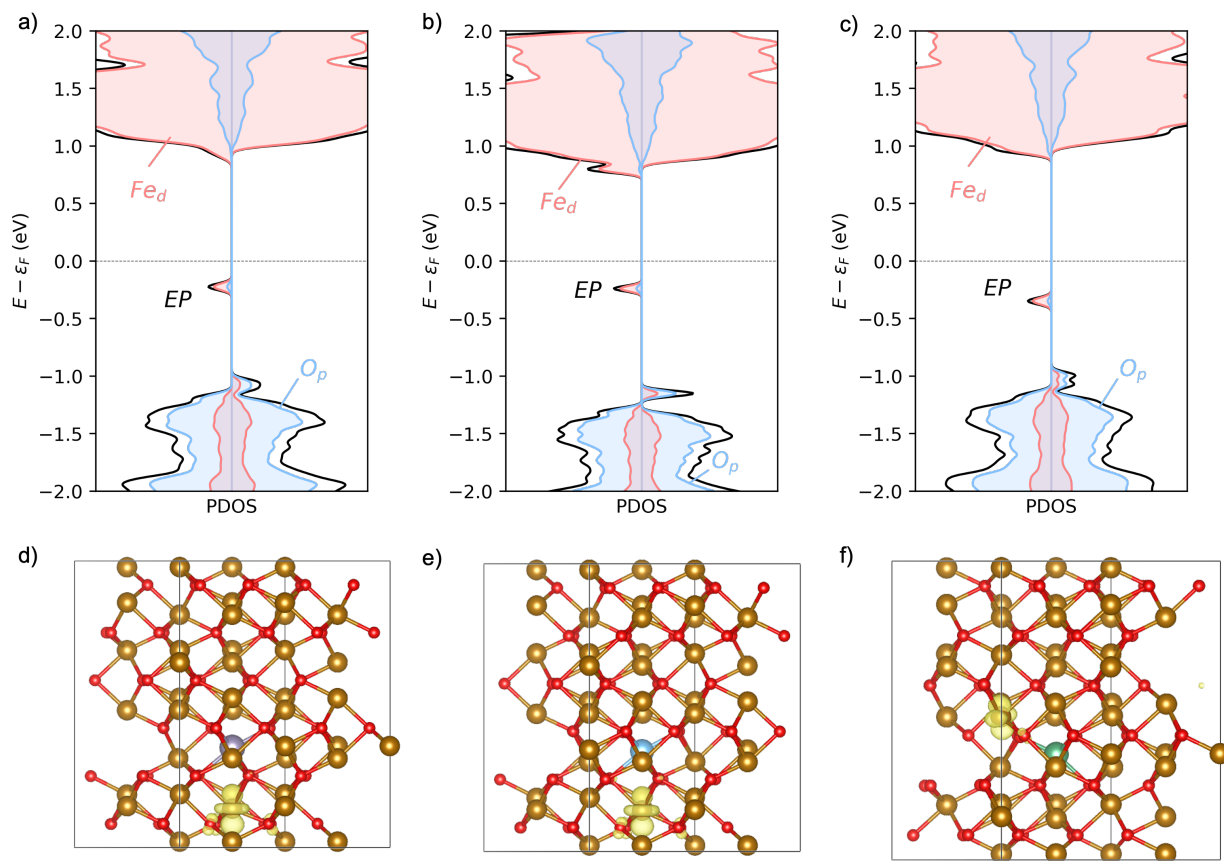


**Figure S16.** a-c) Projected density of states (PDOS) for Sn ( $q=0$ ) (a), Ti ( $q=0$ ) (b), and Nb ( $q=+1$ ) (c), doped hematite with localized polaron indicated by *EP*. Only O 2p states and Fe 3d states are marked as other states have minimum contribution in this energy window. (d-f) The module square of polaron wave-function with an isosurface level of 1% of its maximum value, gold atoms represent Fe and red represent O, third color indicates dopant: Sn (d), Ti (e), and Nb (f). Note: The Nb case is the +1 charged systems resulting in one polaron; Sn and Ti doped ones are neutral systems (one polaron generated from the dopant) for fair comparison.

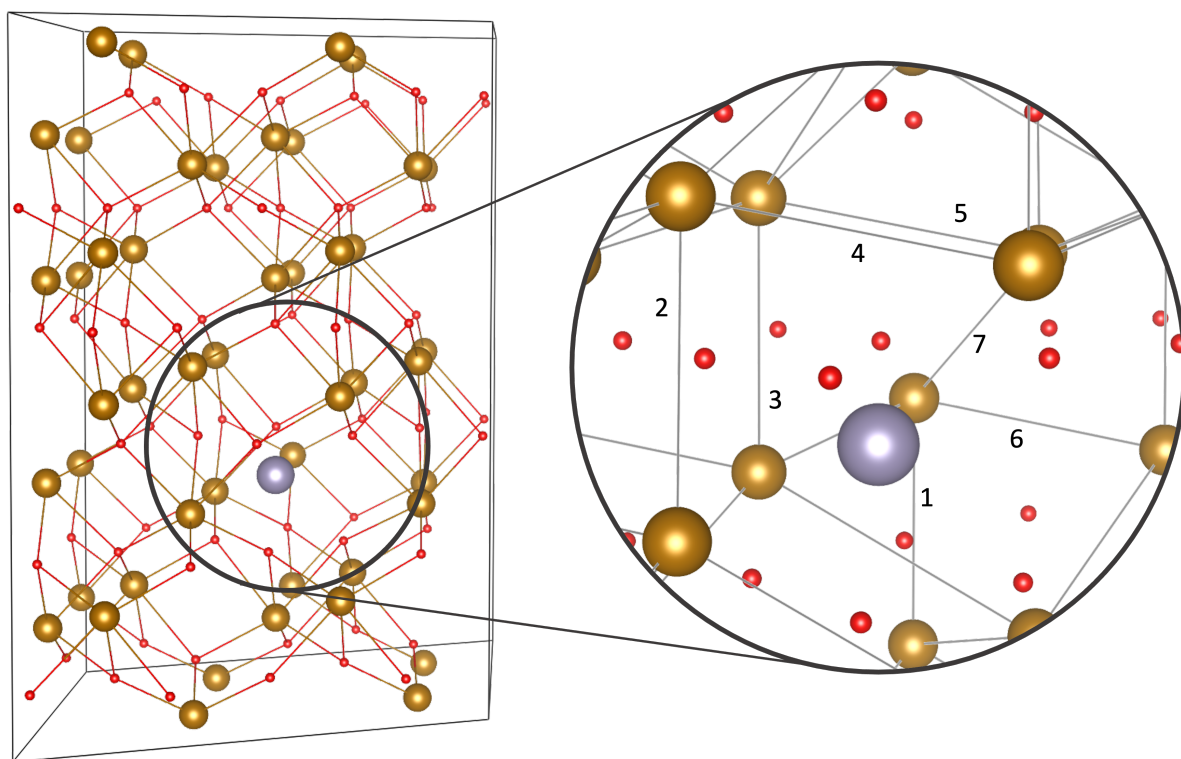


**Figure S17.** Atomic structure of Hematite with Fe in gold and O in red. Left image has Fe-O bonds while the zoomed cutout has visualization of bonds; instead Fe-Fe pairs are connected with selected pairs enumerated as a reference for distances listed in Table S6.

**Table S6.** Fe-Fe pair distances in Å of the enumerated Fe-Fe pair distances in Fig. S17 for pristine and doped systems.

Fe-Fe Pair	Pristine	Sn	Ti	Nb
1	2.92425	2.93833	2.93121	2.94264
2	2.92425	2.95802	2.96007	2.99290
3	2.92425	2.95802	2.96007	2.99282
4	3.01816	3.02057	3.00607	3.10813
5	3.01816	3.06271	3.06628	3.00972
6	3.01822	3.00365	3.01169	3.00036
7	3.43245	3.44309	3.44499	3.40413

## References

- (1) Wu, F.; Ping, Y. Combining Landau–Zener theory and kinetic Monte Carlo sampling for small polaron mobility of doped  $\text{BiVO}_4$  from first-principles. *Journal of Materials Chemistry A* **2018**, *6*, 20025–20036.
- (2) Ling, Y.; Wang, G.; Wheeler, D. A.; Zhang, J. Z.; Li, Y. Sn-doped hematite nanostructures for photoelectrochemical water splitting. *Nano letters* **2011**, *11*, 2119–2125.
- (3) Smart, T. J.; Baltazar, V. U.; Chen, M.; Yao, B.; Mayford, K.; Bridges, F.; Li, Y.; Ping, Y. Doping bottleneck in hematite: Multipole clustering by small polarons. *Chemistry of Materials* **2021**, *33*, 4390–4398.
- (4) Booth, C. H. R-Space X-ray Absorption Package, 2010. 2010; <http://lise.lbl.gov/R SXAP/>.
- (5) Ankudinov, A. L.; Rehr, J. J. Relativistic calculations of spin-dependent x-ray-absorption spectra. *Phys. Rev. B* **1997**, *56*, R1712–R1715.
- (6) Adelstein, N.; Neaton, J. B.; Asta, M.; De Jonghe, L. C. Density functional theory based calculation of small-polaron mobility in hematite. *Physical Review B* **2014**, *89*, 245115.